

# Analysis and Control of a Cellular Converter System with Stochastic Ripple Cancellation and Minimal Magnetics

David J. Perreault, *Student Member, IEEE*, and John G. Kassakian, *Fellow, IEEE*

**Abstract**—A parallel converter architecture based on the resonant pole inverter (RPI) topology is presented. It is shown that this architecture minimizes the output magnetics required for current sharing. A new current control scheme is introduced which reduces peak currents, losses, and output voltage ripple for many operating conditions. This new control method is applicable to both the single RPI and the parallel architecture. Additionally, the paper analytically quantifies the degree of passive ripple cancellation between cells of a parallel architecture. It is shown that the rms ripple current of an  $N$ -cell paralleled converter system is a factor of  $1/\sqrt{N}$  lower than for an equivalent single converter. These results are verified using a piecewise-linear model. We conclude that the parallel architecture overcomes some of the major disadvantages of the conventional RPI.

## I. INTRODUCTION

CONSTRUCTION of high power converter systems by paralleling many low-power converter cells has substantial potential advantages over conventional single large converter designs. Advantages of such cellular converter architectures include performance, reliability, modularity, manufacturability, cost, and the ability to switch at higher frequencies [1], [2]. While paralleled converter systems are often used at very high power levels [3]–[5], and in those applications which demand high reliability [6], the rating of the paralleled converters has been too large to permit mass production manufacturing techniques and high-frequency switching.

Realizing the benefits of a cellular architecture requires suitable converter topologies and control techniques. This paper discusses some key issues in the design of cellular converter systems and presents a new parallel architecture implementation which addresses these design issues. We show that this architecture mitigates some of the major drawbacks of the single resonant pole inverter (RPI) on which it is based. Furthermore, we present an enhanced control algorithm applicable to both the RPI and the parallel architecture which significantly reduces converter stresses and losses for many operating conditions.

Another contribution of the paper is the analysis of the passive ripple cancellation which occurs among cells in a parallel architecture. We show that a  $1/\sqrt{N}$  reduction in rms

output ripple current is expected when paralleled converters are controlled autonomously (e.g., without interleaving). This analytical result is corroborated via piecewise simulation of the new parallel architecture.

## II. CURRENT SHARING

Constructing a large converter by paralleling smaller converter cells requires a current sharing mechanism to prevent the destructive overload of individual cells. Current sharing can be achieved by using an appropriate control scheme in conjunction with a magnetic structure which absorbs the instantaneous voltage differences between cells. Stated another way, the individual cells should be made to behave as current sources for times on the order of the switching period.

The interphase transformer (IPT) is the standard structure for paralleling two converters [3], [7], [8], and can be extended to more converter cells using many legged IPT's [9], [10] or whiffletree connections of IPT's [10], [11]. However, these designs are inappropriate for paralleling large numbers of cells because they are difficult to manufacture, and the cells cannot be made autonomous (an important condition for increased system reliability). Another approach is to place an inductor at the output of each bridge leg [4], [12], [13]. This structure results in a converter system which is modular and more manufacturable. However, the size of the output inductor is an important design parameter, since it can represent an appreciable fraction of converter size and cost. Minimization of the energy storage requirement of the output inductor is thus a key design goal for a practical cellular architecture.

## III. SIZING OF BRIDGE OUTPUT INDUCTANCE

Consider the single-phase half-bridge converter of Fig. 1 operating under hysteretic current control. The converter is loaded by a voltage source  $v_o$ , which, for times on the order of the switching period, represents the output filter, the load, and other paralleled cells. Given a maximum switching frequency  $f_{sw}$ , a reference current  $i_{ref}$ , and a specified hysteresis band  $\Delta i_{band}$ , the energy storage requirement of the inductor is

$$W_t = \frac{i_{ref} V_{dc} (1+k)^2}{16 f_{sw} k} \quad (1)$$

Manuscript received October 30, 1995; revised June 21, 1996. This work was supported by the Bose Foundation.

The authors are with the Massachusetts Institute of Technology, Laboratory for Electromagnetic and Electronic Systems, Cambridge, MA 02139 USA.

Publisher Item Identifier S 0885-8993(97)00422-5.

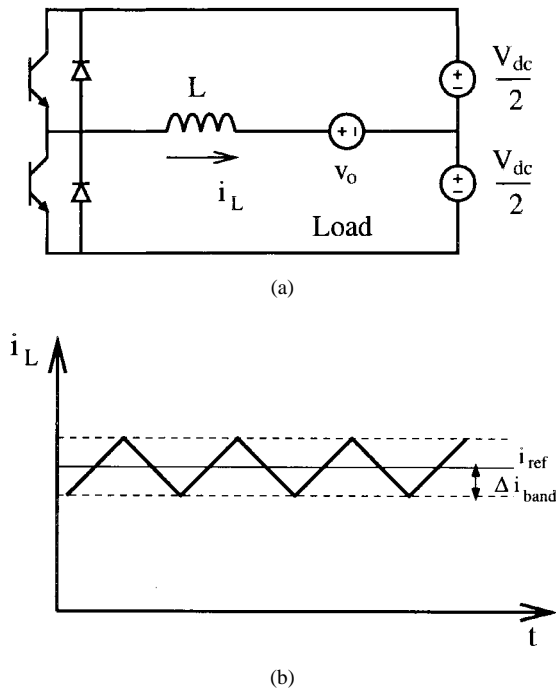


Fig. 1. (a) A half-bridge current-controlled inverter and (b) its output current waveform.

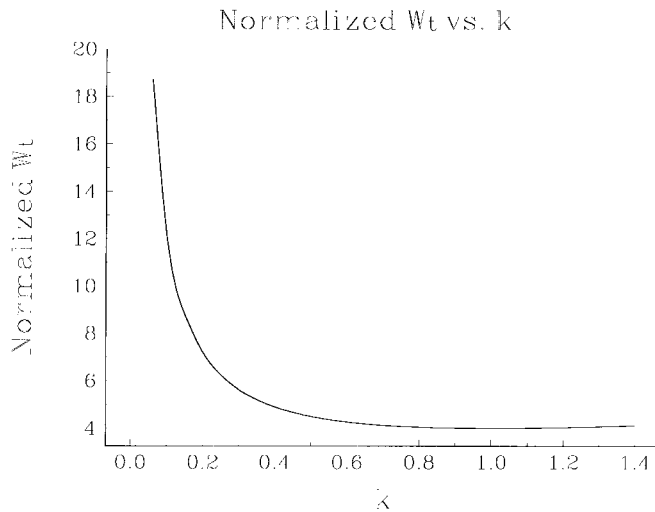


Fig. 2. Output inductor energy storage requirement as a function of ripple ratio,  $k$ .

where  $k = \Delta i_{\text{band}}/i_{\text{ref}}$ . Fig. 2 shows a plot of (1) as a function of  $k$  and shows that the minimum point of this curve is at  $k = 1$ , with only minor costs in increased energy storage for values over one. Operation with a ripple ratio approaching or exceeding one results in the smallest energy storage requirement on the output inductor.

Operation with a large ripple ratio can also be used to obtain soft-switching of the devices. Soft-switched operation is desirable because the reduction of switching losses allows an increase in the switching frequency and a commensurate reduction in component size. As will be shown in the next section, the RPI is a hysteresis-controlled converter which

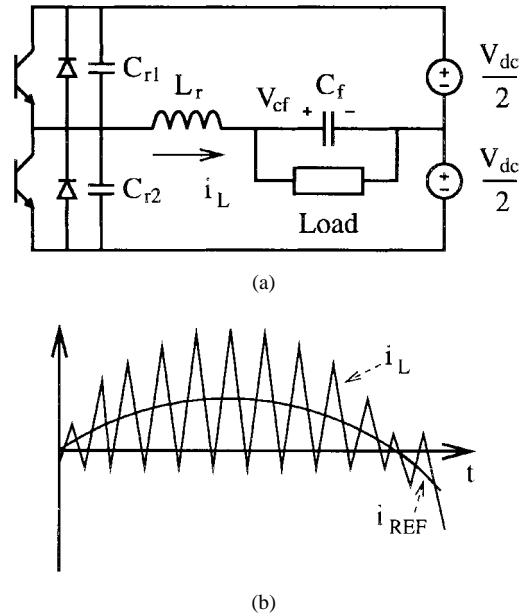


Fig. 3. (a) The RPI and (b) its output current waveform.

maintains zero-voltage switching by operating with a ripple ratio  $k$  slightly greater than one.

#### IV. THE RPI

The RPI converter topology is shown in Fig. 3 [14]–[21]. The operation of this converter is illustrated in Fig. 4 and proceeds as follows. Assume operation begins with  $S_1$  conducting (Mode 1). If the filter capacitor is large enough to clamp the output voltage over the cycle, the inductor current will build up linearly until it reaches a current  $i_{p+}$  determined by the controller. At this point the controller turns  $S_1$  off, and the inductor rings with the two resonant capacitors  $C_{r1}, C_{r2}$  (Mode 2) until  $D_2$  turns on (Mode 3).  $S_2$  is then turned on while  $D_2$  conducts. During this time, the current in the inductor linearly decreases and reverses direction (Mode 4). When the current in the inductor reaches a level  $i_{p-}$ , the controller turns  $S_2$  off, and the inductor rings with the resonant capacitors (Mode 5) until  $D_1$  conducts (Mode 6).  $S_1$  can then be turned on, and the cycle repeats. Note that all switch transitions occur at zero switch voltage.

As with standard hysteresis-based pulse width modulation (PWM), the switching frequency varies dynamically. If the length of the resonant transitions is small and does not affect the inductor current heavily, the instantaneous switching period can be approximated as

$$T \approx \frac{V_{\text{dc}} L_r (i_{p+} + |i_{p-}|)}{\frac{1}{4} V_{\text{dc}}^2 - V_{\text{cf}}^2} \quad (2)$$

The values of  $i_{p+}$  and  $i_{p-}$  used by the controller are constrained by the necessity of having enough energy in the inductor to ring the resonant capacitor voltages between zero and  $V_{\text{dc}}$  to obtain zero-voltage switching. That is, when a device turns off, there must be sufficient current in the inductor to drive the bridge-leg centerpoint voltage to the opposite rail and allow the opposing device to turn on at zero voltage.

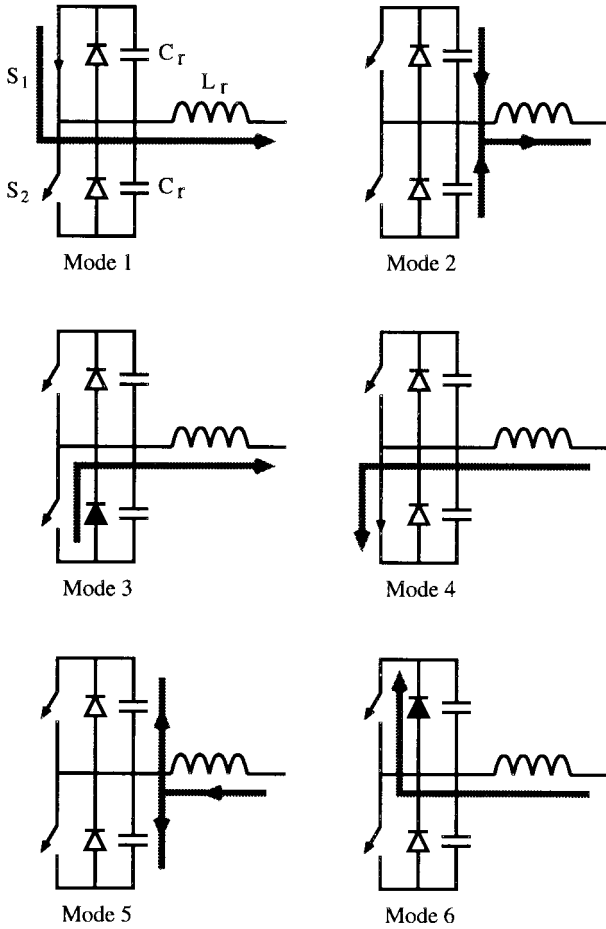


Fig. 4. An operational cycle of the RPI.

Assuming ideal components, a minimum inductor current  $i_{\min}$  is needed at the end of Mode 1 if  $V_{cf} > 0$  where we define

$$i_{\min}(V_{cf}) = 2\sqrt{\frac{C_r V_{dc} |V_{cf}|}{L_r}}. \quad (3)$$

No current is required for  $V_{cf} \leq 0$ . Similarly, the magnitude of  $i_{p-}$  must exceed  $i_{\min}$  at the end of Mode 4 if  $V_{cf} < 0$  and may be zero for  $V_{cf} \geq 0$ .

#### A. Conventional RPI Control

The desired local average output current  $i_{\text{ref}}$  is generated by controlling the values of  $i_{p+}$  and  $i_{p-}$ . If the time spent in the resonant transitions is small and does not severely affect the inductor current, the output current waveform can be treated as triangular, yielding an approximate local average output current of  $(i_{p+} + i_{p-})/2$ . The conventional control method for generating a desired  $i_{\text{ref}}$  is shown in Table I. This method ensures that the inductor current is high enough at each transition by adding a margin  $i_m$  to the magnitude of both  $i_{p+}$  and  $i_{p-}$ , where  $i_m$  is a current sufficiently greater than  $i_{\min}$  to ensure reliable operation.

#### B. Enhanced RPI Control

While the conventional control approach is simple and always ensures that the resonant inductor current constraints

 TABLE I  
 CONVENTIONAL RPI CONTROL

$i_{\text{ref}}$	$< 0$	$> 0$
	$i_{p+} = i_z$ $i_{p-} = 2i_{\text{ref}} - i_z$ $i_z = i_m$	$i_{p+} = 2i_{\text{ref}} + i_z$ $i_{p-} = -i_z$ $i_z = i_m$

 TABLE II  
 ENHANCED RPI CONTROL

$i_{\text{ref}}$	$< 0$	$> 0$
$V_{cf} > 0$	$i_{p+} = i_z$ $i_{p-} = 2i_{\text{ref}} - i_z$ $i_z = i_m$	$i_{p+} = 2i_{\text{ref}} + i_z$ $i_{p-} = -i_z$ $i_z = \max(i_m - 2i_{\text{ref}}, 0)$
$V_{cf} < 0$	$i_{p+} = i_z$ $i_{p-} = 2i_{\text{ref}} - i_z$ $i_z = \max(i_m + 2i_{\text{ref}}, 0)$	$i_{p+} = 2i_{\text{ref}} + i_z$ $i_{p-} = -i_z$ $i_z = i_m$

are met, it yields currents which are significantly higher than needed to ensure zero-voltage switching for many operating conditions. This is because the conventional control method always ensures that the magnitudes of  $i_{p+}$  and  $i_{p-}$  exceed  $i_{\min}$  even though this is not necessary for all values of  $V_{cf}$ .

We introduce a new control method, shown in Table II, which reduces peak currents, losses, and output voltage ripple for many operating conditions and yields identical performance for all others. The new control method takes advantage of the fact that for a given output voltage polarity, there is a minimum inductor current requirement for only one of the two resonant transitions. When  $V_{cf} > 0$ , there is only a minimum required value for  $i_{p+}$ , and when  $V_{cf} < 0$ , there is only a minimum value for the magnitude of  $i_{p-}$ . Thus, when we are sourcing power from the converter (quadrants one and three), we need only supply any difference between the peak current needed to source  $i_{\text{ref}}$  alone and that required for the resonant transition. In quadrants three and four, we are left with the conventional control method. The control method shown in Table II achieves this and is simple to implement in analog hardware.

To illustrate the benefits of this enhanced control technique, we consider the simulation results shown in Fig. 5. The half bridge converter in this example is used to drive an RL load at 65 V and 60 Hz. For both control methods, the system has an outer PI voltage control loop yielding a sinusoidal output voltage and uses a value of  $i_m = i_{\min}(V_{cf})$  with an additional constant safety margin for peak current calculations. The resonant inductor current is significantly reduced for the enhanced method as are the device and filter capacitor currents. For the example shown, the rms current of the filter capacitor was reduced by over 15% compared to the conventional method. This benefit of the enhanced control algorithm is especially significant for converters which operate at partial load since it improves partial-load efficiency by reducing the fixed losses associated with maintaining zero-voltage switching.

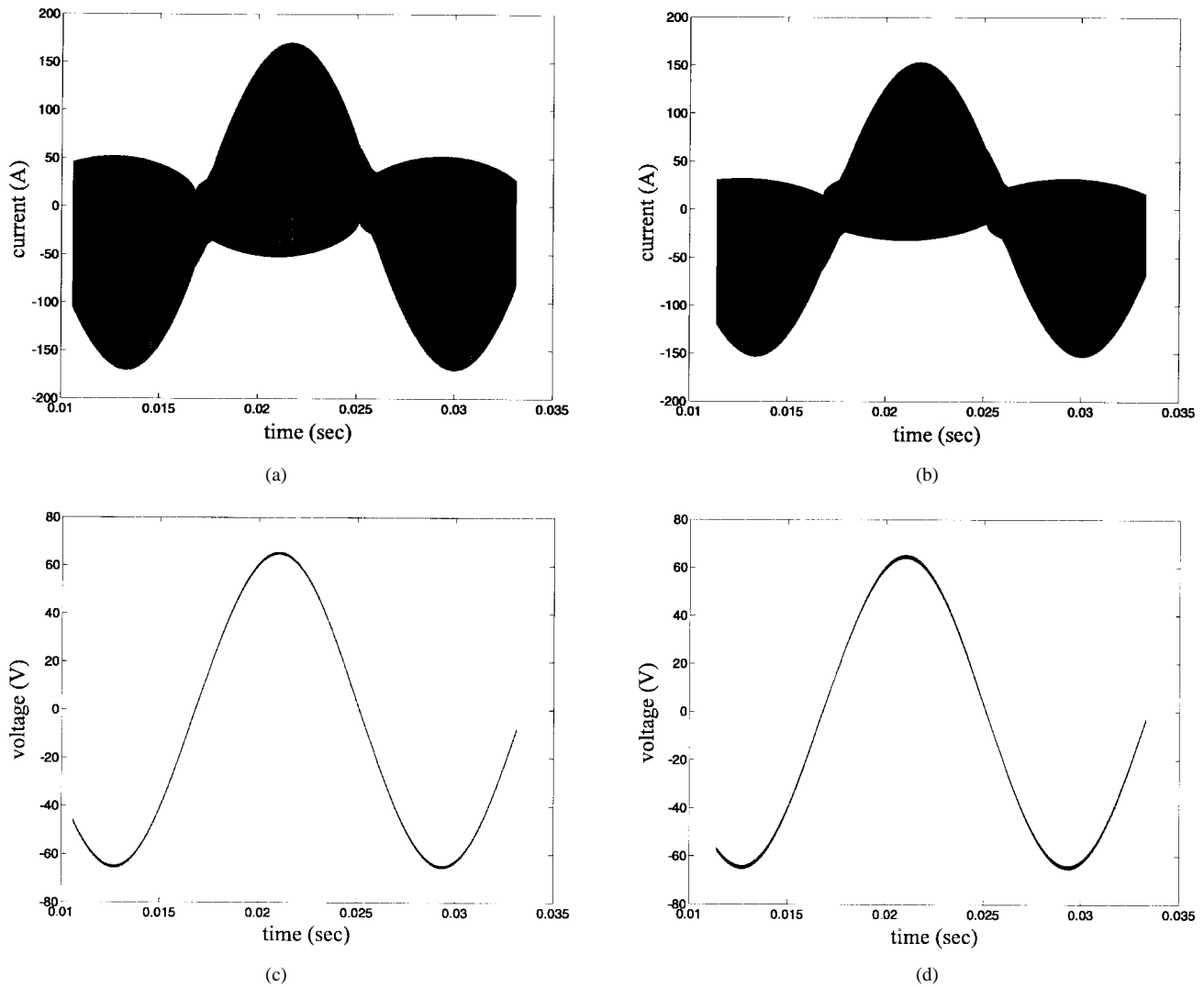


Fig. 5. Comparison of RPI control methods. RPI has  $L_r = 15 \mu\text{H}$ ,  $C_r = 0.16 \mu\text{F}$ ,  $C_f = 150 \mu\text{F}$ ,  $L_l = 1 \text{ mH}$ ,  $R_l = 1 \Omega$ , and  $V_{dc} = 300 \text{ V}$ .

One minor disadvantage of the enhanced control method is that the approximate relationship among  $i_{ref}$ ,  $i_{p+}$ , and  $i_{p-}$  is less accurate for the enhanced method than for the conventional method. Because the currents are lower for the enhanced method, more time is spent in the resonant transitions, and the overall waveform shape is affected more by the transitions. However, these effects are easily compensated for using feedback and do not pose a significant problem as can be seen by the resulting waveform quality in Fig. 5.

## V. THE PARALLEL RESONANT POLE INVERTER

An important contribution of this paper is the development of the parallel RPI (PRPI) architecture based on the RPI cell structure, as shown in Fig. 6. For simplicity, the single-phase half-bridge will be discussed here. Constructing a parallel system using RPI cells meets the objective of minimizing the size of the magnetic structure since the RPI cells operate near the minimum energy storage point of (1). Furthermore, because this converter is fully soft-switched, it can operate at higher frequencies than a comparable hard-switched converter for the same total losses. This increase in switching frequency further

reduces the size of the required magnetic components according to (1). These advantages are achieved with a minimum of added components and a simple control system. We will also show that significant ripple reduction occurs due to stochastic cancellation in the aggregated output of the cells.

### A. PRPI Advantages

In addition to its other attributes, the PRPI eliminates two of the major drawbacks of the conventional RPI. As discussed in [16], the practical size of an RPI is limited by the difficulty of constructing output inductors of a large enough rating. However, an  $N$  cell PRPI can be constructed which is functionally equivalent to a single RPI of  $N$  times the cell VA rating, increasing the converter size by a factor of  $N$  over that achievable using a single RPI. To see this, consider breaking down a single RPI into  $N$  cells as shown in Fig. 7. Each of these converter cells will, to first order, operate at the same frequency as the original and have  $1/N$  times the losses. Thus, creating the same VA rating with equivalent parallel cells distributes the inductance in a manner which makes it far more manufacturable than a single large converter. This benefit is in

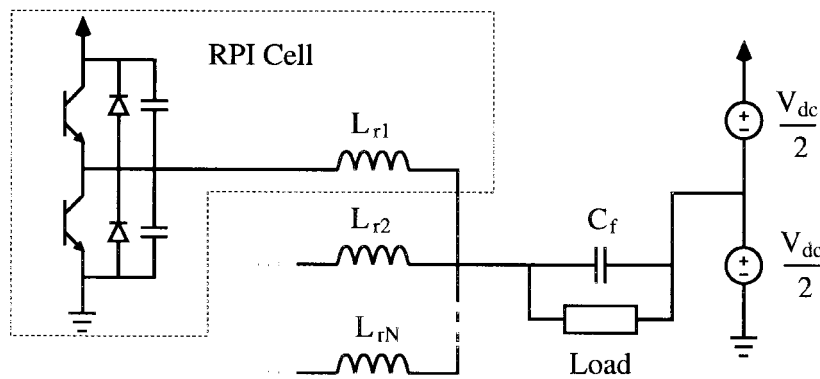


Fig. 6. The PRPI architecture.

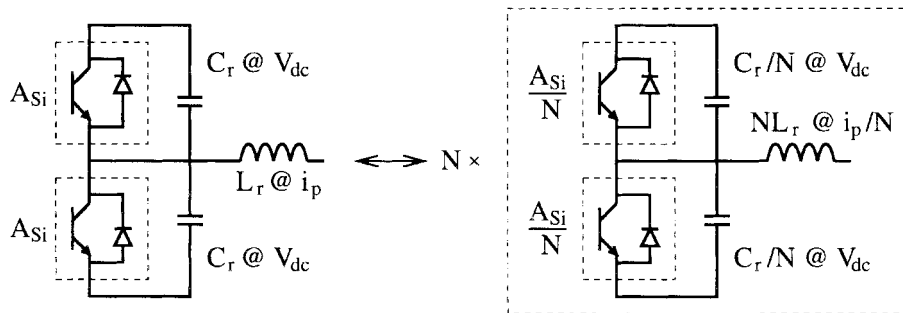


Fig. 7. An RPI leg and its equivalent parallel resonant pole components.

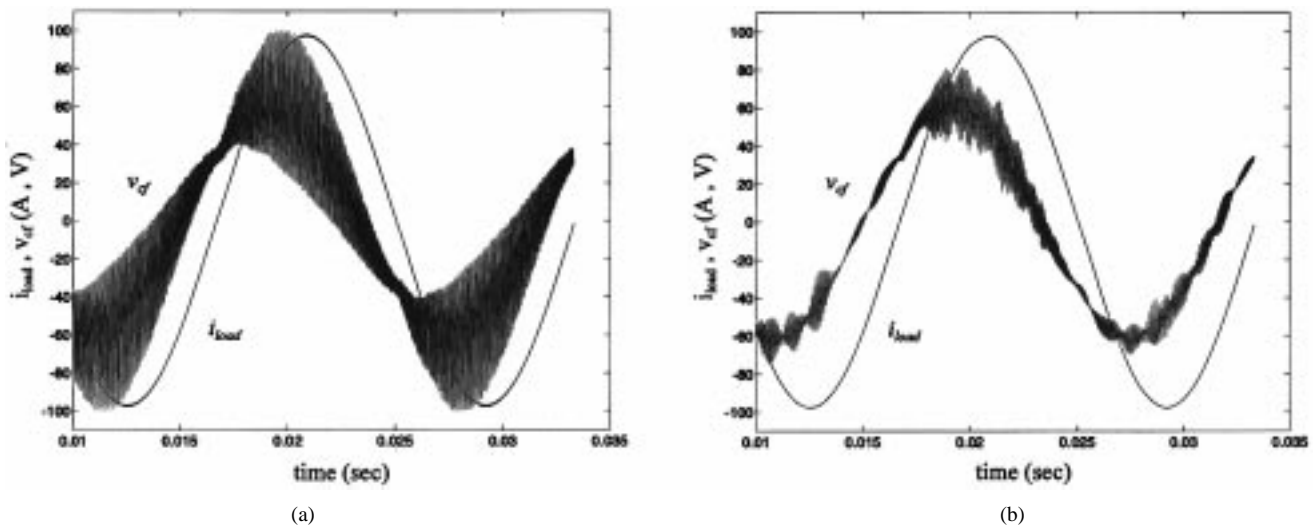


Fig. 8. (a) Comparison of output voltage and current for a single RPI and (b) an equivalent ten-cell PRPI system. The single RPI has  $L_r = 25 \mu\text{H}$ ,  $C_r = 0.16 \mu\text{F}$ ,  $C_f = 50 \mu\text{F}$ ,  $L_{\text{load}} = 1 \text{ mH}$ , and  $R_{\text{load}} = 1 \Omega$ .

addition to the fact that, in practice, the smaller converters can be designed to operate at higher frequencies than a single large converter due to reduction of parasitics and the distribution of heat generation [2].

Another major difficulty with RPI's is the high current ratings of the output filter capacitors [17]. Ripple cancellation among the individual converters of a PRPI significantly

reduces the rms current stress on the filter capacitors, even when the cells are controlled autonomously (without active ripple cancellation). We compare the relative performances of a single RPI and a ten-cell PRPI, both operating under the enhanced control method described previously, as shown in Fig. 8. The simulation results, obtained using the piecewise model of Appendix A, show that the rms current stress on

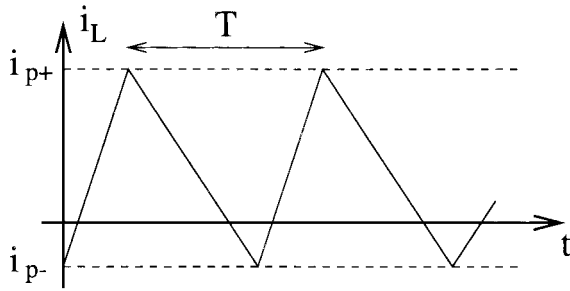


Fig. 9. The RPI inductor current waveform at a fixed operating point.

the PRPI filter capacitor is over 70% less than that in the equivalent single RPI, and the voltage ripple is lower as well. This reduction is purely due to ripple cancellation among the outputs of the cells and is likely to be useful for diminishing acoustic noise and EMI.

## VI. ANALYSIS OF PASSIVE RIPPLE CANCELLATION

A significant contribution of this paper is the quantification of the amount of passive or *stochastic* ripple cancellation which occurs between paralleled cells in a cellular architecture. We will show that if a single large RPI is replaced by an equivalent  $N$ -cell PRPI, a  $1/\sqrt{N}$  reduction in rms output ripple current is expected under open-loop conditions when the cells are controlled autonomously (no active ripple cancellation).

Consider a single RPI with parameters  $L_r$  and  $C_r$  operating at a fixed output voltage  $v_{cf}$  and commanded current  $i_{ref}$ . The inductor current waveform of Fig. 9 is periodic with a period  $T$  determined by (2) and has peak currents

$$\begin{aligned} i_{p+} &= 2i_{ref} + i_m \\ i_{p-} &= -i_m. \end{aligned} \quad (4)$$

The output ripple current  $i_x$  is equal to the inductor current  $i_L$  minus its dc level. We can express the ripple current as a Fourier series

$$i_x = \sum_{n=-\infty}^{\infty} C_n e^{jn\omega_o t} \quad (5)$$

where

$$\omega_o = \frac{2\pi}{T}. \quad (6)$$

The power spectral density of the ripple current is then

$$S_{i_x}(\omega) = 2\pi \sum_{n=-\infty}^{\infty} |C_n|^2 \delta(\omega - n\omega_o). \quad (7)$$

This yields an rms ripple current value of

$$i_{x,rms} = \sqrt{\frac{1}{2\pi} \int_{-\infty}^{+\infty} S_{i_x}(\omega) d\omega} = \sqrt{\sum_{n=-\infty}^{\infty} |C_n|^2}. \quad (8)$$

Now we break down the single RPI into an equivalent  $N$ -cell PRPI as shown in Fig. 7 where the  $k$ th cell has parameters

$$\begin{aligned} C_{r,k} &\approx \frac{C_r}{N} \\ L_{r,k} &\approx N L_r. \end{aligned} \quad (9)$$

For these parameters, we find

$$\begin{aligned} i'_{p+} &= 2\frac{i_{ref}}{N} + \frac{i_m}{N} \\ i'_{p-} &= -\frac{i_m}{N} \end{aligned} \quad (10)$$

and a switching period of the  $k$ th cell of approximately

$$T_k \approx \frac{V_{dc} L_{r,k} (i'_{p+} + |i'_{p-}|)}{\frac{1}{4} V_{dc}^2 - V_{cf}^2}. \quad (11)$$

The output current waveforms of the cells are essentially  $1/N$  scaled versions of the single RPI output current with small variations in frequency due to deviations of the individual cell parameters from their nominal values.

We can express the output ripple current of an individual PRPI cell as

$$i'_{rip,k} = \sum_{n=-\infty}^{\infty} C_{k,n} e^{jn\omega_k t} \quad (12)$$

where

$$\omega_k = \frac{2\pi}{T_k} \quad (13)$$

and

$$C_{k,n} \approx \frac{C_n}{N}. \quad (14)$$

The power spectral density of the  $k$ th cell output ripple current is

$$S_{i'_{rip,k}}(\omega) = 2\pi \sum_{n=-\infty}^{\infty} |C_{k,n}|^2 \delta(\omega - n\omega_k). \quad (15)$$

Because the  $T_k$ 's are not identical due to parameter variations among the cells (including resonant component values, sensor gains, etc.), the power spectral density of the total ripple current is the sum of the power spectral densities of the individual cell ripple currents. Thus, for the PRPI case, the power spectral density of the total ripple current is

$$\begin{aligned} S_{i'_x}(\omega) &= 2\pi \sum_{k=1}^N \sum_{n=-\infty}^{\infty} |C_{k,n}|^2 \delta(\omega - n\omega_k) \\ &\approx \frac{2\pi}{N^2} \sum_{k=1}^N \sum_{n=-\infty}^{\infty} |C_n|^2 \delta(\omega - n\omega_k). \end{aligned} \quad (16)$$

This leads to an rms ripple current of

$$\begin{aligned} i'_{x,rms} &= \sqrt{\frac{1}{2\pi} \int_{-\infty}^{+\infty} S_{i'_x}(\omega) d\omega} \approx \sqrt{\frac{1}{N} \sum_{n=-\infty}^{\infty} |C_n|^2} \\ &\approx \frac{i_{x,rms}}{\sqrt{N}}. \end{aligned} \quad (17)$$

Hence, if a single large RPI is replaced by an equivalent  $N$ -cell PRPI, a  $1/\sqrt{N}$  reduction in rms output ripple current is expected when the converters are controlled autonomously.

To verify this result, the RPI example of Fig. 8 was simulated over one line cycle using the method of Appendix A, and the rms ripple current was calculated. This was repeated

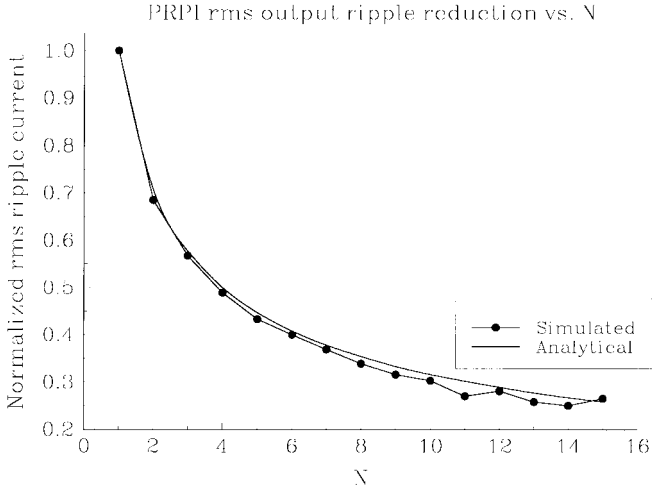


Fig. 10. Theoretical and simulated reductions in rms current ripple versus  $N$  for the PRPI.

for equivalent PRPI converters of 2–15 cells. To model the parameter variations occurring in real converters, a uniformly distributed 5% random variation in resonant component values was used. The results of these simulations, plotted in Fig. 10, corroborate the analysis. With slight modifications to the derivation, the result is applicable to a variety of other cell topologies as well.

Thus, the use of a PRPI significantly reduces the requirements on the output filter compared to a single RPI, even when the converters are controlled autonomously. The same ripple cancellation effects can be expected under closed-loop conditions, providing that the control strategy does not induce sympathetic synchronism between individual cells. Interdependent current control of the cells or locally controlled ripple cancellation schemes would further improve the advantage of the PRPI.

## VII. CONCLUSION

The paper describes a new parallel converter architecture based on the resonant pole circuit topology. It is shown that the architecture meets the important objective of minimizing the required output magnetics while retaining the simplicity of the basic bridge structure. Furthermore, we show that the approach mitigates some of the major drawbacks of the single RPI.

A novel current control scheme applicable to both the new parallel architecture and the single RPI is also introduced. This control scheme significantly reduces converter losses and stresses under many operating conditions compared to the conventional control method.

Finally, the paper analytically quantifies the amount of passive ripple cancellation which occurs among cells in a parallel architecture. We show that a  $1/\sqrt{N}$  reduction in total rms ripple current is expected when  $N$  autonomously controlled converters are paralleled. This important result is corroborated via piecewise simulation of the new parallel architecture.

## APPENDIX A MODELING OF THE PRPI

This appendix presents a piecewise model for simulating the general  $N$ -converter PRPI system of Fig. 6. The model assumes ideal switches and components and an  $R$ - $L$ - $E$  load. We give state equations for the resonant inductor current and (bottom) capacitor voltage of the  $k$ th converter cell in each mode along with the boundary conditions for transition to the next mode. State equations valid under all conditions are presented for the filter capacitor voltage and load current. The resonant inductor current and bottom resonant capacitor voltage of the  $k$ th converter cell are denoted as  $i_{L,k}$  and  $v_{C,k}$ , respectively.

The state equations for the filter capacitor voltage,  $v_{cf}$ , and load current,  $i_l$ , are

$$\frac{dv_{cf}}{dt} = \frac{\left(\sum_{k=1}^N i_{L,k}\right) - i_l}{C_f} \quad (18)$$

$$\frac{di_l}{dt} = \frac{v_{cf} - i_l R - E}{L_l}. \quad (19)$$

The equations for the  $k$ th converter in Mode 1 or 6 ( $S_1/D_1$  on,  $S_2/D_2$  off) are

$$\frac{di_{L,k}}{dt} = \frac{\frac{1}{2} V_{dc} - v_{cf}}{L_{r,k}} \quad (20)$$

$$\frac{dv_{C,k}}{dt} = 0. \quad (21)$$

This mode is valid until the inductor current reaches the specified value ( $i_{p+}$ ), and  $S_1$  is turned off.

For the  $k$ th converter in Mode 2 ( $S_1/D_1$  off,  $S_2/D_2$  off, top to bottom transition)

$$\frac{dv_{C,k}}{dt} = -\frac{i_{L,k}}{2C_{r,k}} \quad (22)$$

$$\frac{di_{L,k}}{dt} = \frac{v_{C,k} - \frac{1}{2} V_{dc} - v_{cf}}{L_{r,k}}. \quad (23)$$

This mode is valid while  $v_{C,k} > 0$ .

For the  $k$ th converter in Mode 3 or 4 ( $S_1/D_1$  off,  $S_2/D_2$  on)

$$\frac{di_{L,k}}{dt} = \frac{-\frac{1}{2} V_{dc} - v_{cf}}{L_{r,k}} \quad (24)$$

$$\frac{dv_{C,k}}{dt} = 0. \quad (25)$$

This mode is valid until the inductor current reaches the specified value and  $S_2$  is turned off.

For the  $k$ th converter in Mode 5 ( $S_1/D_1$  off,  $S_2/D_2$  off, bottom to top transition)

$$\frac{dv_{C,k}}{dt} = -\frac{i_{L,k}}{2C_{r,k}} \quad (26)$$

$$\frac{di_{L,k}}{dt} = \frac{v_{C,k} - \frac{1}{2} V_{dc} - v_{cf}}{L_{r,k}}. \quad (27)$$

This mode is valid while  $v_{C,k} < V_{dc}$ .

The relevant state equations are solved at each time step, changing the modes of the individual converters as necessary.

## ACKNOWLEDGMENT

D. Perreault acknowledges the support of an IEEE Convergence Fellowship in Transportation Electronics.

## REFERENCES

- [1] J. Kassakian, "High frequency switching and distributed conversion in power electronic systems," presented at the Sixth Conf. Power Electronics Motion Control (PEMC '90), Budapest, Hungary, 1990.
- [2] J. Kassakian and D. Perreault, "An assessment of cellular architectures for large converter systems," in *Proc. First Int. Power Electronics Motion Control Conf.*, Beijing, China, 1994, pp. 70–79.
- [3] M. Honbu, Y. Matsuda, K. Miyazaki, and Y. Jifuku, "Parallel operation techniques of GTO inverter sets for large ac motor drives," in *IEEE IAS Annu. Meeting*, 1982, pp. 657–662.
- [4] M. Hashii, K. Kousaka, and M. Kaimoto, "New approach to a high power GTO PWM inverter for ac motor drives," in *IEEE IAS Annu. Meeting*, 1985, pp. 467–472.
- [5] S. Tadakuma, S. Tanaka, K. Miura, H. Inokuchi, and H. Ikeda, "Fundamental approaches to PWM control based GTO inverters for linear synchronous motor drives," in *IEEE IAS Annu. Meeting*, 1991, pp. 847–853.
- [6] J. Holtz, W. Lotzkatz, and K. Werner, "A high-power multitransistor-inverter uninterruptible power supply system," *IEEE Trans. Power Electron.*, vol. 3, no. 3, pp. 278–285, July 1988.
- [7] S. Okuma, K. Iwata, and K. Suzuki, "Parallel running of GTO PWM inverters," in *IEEE Power Electronics Specialists Conf.*, 1984, pp. 111–120.
- [8] S. Ogasawara, J. Takagaki, H. Akagi, and A. Nabae, "A novel control scheme of a parallel current-controlled PWM inverter," *IEEE Trans. Ind. Applicat.*, vol. 28, no. 5, pp. 1023–1030, Sept./Oct. 1992.
- [9] J. Schaefer, *Rectifier Circuits: Theory and Design*. New York: Wiley, 1965, pp. 49–51.
- [10] P. Wood, *Switching Power Converters*. New York: Van Nostrand, 1981, pp. 61–66.
- [11] K. Matsui, Y. Murai, M. Watanabe, M. Kaneko, and F. Ueda, "A pulsewidth modulated inverter with parallel-connected transistors using current sharing reactors," *IEEE Trans. Power Electron.*, vol. 8, no. 2, pp. 186–191, Apr. 1993.
- [12] M. Youn and R. Hoft, "Analysis of parallel operation of inverters," in *IEEE IAS Annu. Meeting*, 1976, pp. 951–958.
- [13] F. Petruzzello, P. Ziogas, and G. Joos, "A novel approach to paralleling of power converter units with true redundancy," in *IEEE Power Electronics Specialists Conf.*, 1990, pp. 808–813.
- [14] D. Divan and G. Skibinski, "Zero switching loss inverters for high power applications," in *IEEE IAS Annu. Meeting*, 1987, pp. 627–634.
- [15] R. DeDoncker, D. Divan, and T. Lipo, "High power soft switching inverters," in *PESC '91 Tutorial*, 1991.
- [16] B. Acharya, R. Gascoigne, and D. Divan, "Active power filters using resonant pole inverters," in *IEEE IAS Annu. Meeting*, 1989, pp. 967–973.
- [17] D. Divan and G. Venkataramanan, "Comparative evaluation of soft switching inverter topologies," in *1991 European Power Electronics Conf. (EPE)*, 1991, pp. 2013–2018.
- [18] D. Divan, G. Venkataramanan, and R. DeDoncker, "Design methodologies for soft switched inverters," *IEEE Trans. Ind. Applicat.*, pp. 126–135, Jan./Feb. 1993.
- [19] J. Ferreira and J. Van Wyk, "Component loss modeling in hard switched and resonant pole inverters," in *IEEE IAS Annu. Meeting*, 1991, pp. 1462–1467.
- [20] J. G. Cho, D. Y. Hu, and G. H. Cho, "Three phase sine wave voltage source inverter using the soft switched resonant poles," in *IEEE Industrial Electronics Conf. (IECON)*, 1989, pp. 48–53.
- [21] D. Perreault, H. Martin, R. Selders, and J. Kassakian, "Loss modeling and component selection for resonant pole inverters," in *Proc. 29th Universities Power Engineering Conf. 1994*, pp. 622–625.
- [22] D. Perreault, J. Kassakian, and H. Martin, "A soft-switched parallel inverter architecture with minimal output magnetics," in *1994 IEEE Power Electronics Specialists Conf.*, pp. 970–977.



**David J. Perreault** (S'91) was born in North Providence, RI, on January 22, 1967. He received the B.S. degree from Boston University, MA, in 1989, and the S.M. degree from the Massachusetts Institute of Technology (MIT), Cambridge, in 1991, both in electrical engineering.

He is currently a Ph.D. candidate at MIT and a Research Assistant in the MIT Laboratory for Electromagnetic and Electronic Systems where he is engaged in the research and development of cellular power electronic architectures.

Mr. Perreault is a member of Tau Beta Pi and the National Society of Professional Engineers. He was the recipient of an IEEE Convergence Fellowship in transportation electronics.



**John G. Kassakian** (S'65–M'73–SM'80–F'89) received the Sc.D degree from the Massachusetts Institute of Technology (MIT), Cambridge, in 1973.

He is a Professor of Electrical Engineering and Director of the MIT Laboratory. His fields of expertise are power electronics and automotive electrical systems, and he serves as a Consultant to government and industry. He has published extensively in the area of power electronics and is a coauthor of the textbook *Principles of Power Electronics*.

Dr. Kassakian was the Founding President of the IEEE Power Electronics Society and serves as the U.S. representative to the European Power Electronics Society. He is also a Member of the Board of Directors for several companies. He is the recipient of the IEEE Centennial Medal, the IEEE William E. Newell Award, the IEEE Distinguished Lectureship Award, and the Distinguished Service Award. In 1993, he was elected to the National Academy of Engineering.